J. Chem. & Cheml. Sci. Vol.3 (1), 13-30 (2013)

Kinetics and Mechanism of Thermal Decomposition of Binary Mixture of Barium Oxalate and Ferrous Oxalate in The (1:1) Mole Ratio

SUNITA ZAWARE and SHRIDHAR JADHAV

Department of Chemistry,
New Arts, Commerce and Science College,
Ahmednagar-414001, M. S., INDIA.

(Received on: December 10, 2012)

ABSTRACT

The non- isothermal decomposition study of individual $BaC_2O_4.0.6H_2O$ by TGA technique shows three steps with $BaCO_3$ and BaO as final product when heated to 1000 ^{0}C with three dimensional diffusion (D_4) and two dimensional phase boundary reaction ($R_2\alpha$) mechanism. The energy of activation (Ea) of non-isothermal method is 36.80 KJ/mole and isothermal method is 34.09 KJ/mole. While $FeC_2O_4.2H_2O$ shows two steps decomposition with Fe_2O_3 as final product when heated to 300 ^{0}C with two dimensional diffusion (D_2) and three dimensional diffusion (D_4) mechanism. The Ea by non- isothermal method is 176.33 KJ/mole and isothermal method is 138.33 KJ/mole respectively. The non-isothermal study of the binary mechanical mixture of $BaC_2O_4.0.6H_2O$ and $FeC_2O_4.2H_2O$ in mole ratio (1:1) by TGA when heated up to 1000 ^{0}C shows mixture of BaO and Fe_2O_3. The α Vs time plots of isothermal study of mixture shows Avrami equation ($A_2\alpha$) and three dimensional diffusion (D_3) mechanism. The applicability of three dimensional phase boundary reaction to the kinetic data is up to $0.46 < \alpha < 0.98$. The Ea of this binary mixture in mole ratio (1:1) by non- isothermal method 15.07 KJ/mole and isothermal method is 15.36 KJ/mole. The end products were characterized using X-ray diffraction technique. The kinetic parameters like energy of activation (Ea), pre-exponential factor (A) and Correlation factor (r) were obtained from isothermal TGA and EGA.

Journal of Chemistry and Chemical Sciences, Vol.3, Issue 1, 1 January, 2013 (1-47)

Keywords: FeC_2O_4, BaC_2O_4, TGA, EGA, Kinetics, Oxalates.

1. INTRODUCTION

Thermal decomposition study of metal oxalates is useful for preparation of mixed metal oxides possessing pores, lattice imperfections and therefore they acts as reactive solids [1]. The mixed metal oxides may result in the modification of their thermal behavior, geometry and electronic properties which lead to changes in their catalytic functions [2]. It is found that many workers studied thermal decomposition of mixed metal oxalates preparing them by different techniques [3]. So far, nobody appears to have reported on the thermal behavior of mechanical mixtures of $BaC_2O_4.0.6H_2O$ and $FeC_2O_4.2H_2O$ in (1:1) mole ratio. Generally, the kinetics of solid state thermal decomposition can be followed either by isothermal and non-isothermal methods [4]. In last few years some workers have studied the binary mixtures of oxalates by thermal decomposition to find out the kinetics and mechanism [5-6], but we have chosen quite new method to study the binary mixture by mechanically mixing two oxalates by definite proportion as 1:1, 1:2 ,2:1, 1:3 etc. The effect of mixing on the kinetic parameters of individual oxalates is to be studied. The decomposition in oxalates may be with the heterolytic dissociation of C-C bond forming CO_2 and CO_2^{2-} , if it involves the cleavage of the C-C bond then the products are CO and CO_2. In many cases the C-C bond cleavage is the rate determining step. If cleavage is heterolytic then it produces CO_2 and CO_2^{2-} and if hemolytic then it produces two CO^{2-} anions [7-11]. Non-isothermal thermo-gravimetric analysis (TGA) has been widely used as a tool to investigate the thermal stability of complexes [12]. Thermo-gram obtained, provide the information about the sample composition, thermal stability as well as the kinetic data relating the chemical changes occur on heating [13]. The kinetic parameters of non-isothermal method of TGA and EGA are close to those obtained for isothermal decomposition in the air atmosphere. EGA is known as one of thermal analysis method for measuring the amount of generated gases from a sample as a function of temperature [14]. The kinetic analysis data was performed by using computer for calculation of energy of activation and mechanism. The product remains after thermal decomposition of oxalate mixture was characterized by using X-ray diffraction techniques [15].

2. EXPERIMENTAL

2.1 Material

Pure and Barium (II) oxalate and Ferrous (II) oxalate were used of BDH A.R.quality.

Apparatus

The EGA technique in which furnace is made up of indigenous material with quartz tube closed from one side with chromel-alumel as thermocouple. Pyrometer (Tempo Industrial corp., BPL-INDIA) with range 0 ^{0}C to 1200 ^{0}C (± 1 ^{0}C) and the temperature regulator (Argo transformers Co.Ltd., India) of 15 amp capacity is used. In the non-isothermal studies the temperature was raised up to 1000 ^{0}C at heating rates of ±4 ^{0}C/min. TGA is set up by using thermobalance K-14 super (K. Roy

and Co., India) of 100 g capacity with an accuracy of ± 0.1 mg. The furnace used for TGA is prepared by using indigenous material. The DTA technique Detector DTG-60H where atmosphere is air with flow rate 50 ml/min.

X-ray powder diffraction analysis of the solid decomposition products was carried out using a bruker axs D8 advance X-ray diffractometer. For the identification purpose, the relative intensities (I/I_0) and the d-spacing (Å) were compared with standard diffraction patterns of the ASTM powder diffraction files [16].

2.2 Data Analysis

The activation parameters were then calculated by using the Coats-Redfern equation written in the form:

$$\log_{10}\{1-(1-\alpha)^{1-n}/T^2(1-n\}=\log_{10}AR/aE\ [1-2RT/E]-E/2.303RT \quad (1)$$

Where α = the fraction of the sample decomposed at time t
n = order of reaction
T = temperature (^{0}K)
A= pre-exponential factor
R = gas constant
E = activation energy
a = conversion factor to transfer from a time scale to a temperature scale,

i.e. $a = dT / dt$

In Coats-Redfern equation $\log_{10}AR/aE\ [1-2RT/E]$ remains constant over temperature range of the decomposition, then plot

$\log_{10}\{1-(1-\alpha)^{1-n}/T^2(1-n\}$ against 1 / T

It results straight line and slope give the value of $-E / 2.303\ R$ [17].

For isothermal conditions, the rate expression can be written as

$$G(\alpha) = kt \quad \text{(integral form)} \quad (2)$$

α = the fraction of the sample decomposed at time 't'.

For a given isothermal run at T_i, the constant k (T_i) can be calculated from the TGA and EGA Curve using the integral method. TGA and EGA experiments for isothermal analysis are performed at five isothermal temperatures. There is a certain k (T_i) and certain f (α) or G (α) for each T_i. If f (α) or G (α) are all the same for each T_i, then

$$\ln [G(\alpha) / 1.921503T] = \ln (AE / BR) + 3.7720501 - 1.921503 \ln E - E / RT \quad (3)$$

Where
E = slope x R
And
A = exp (intercept – 3.772051 + 1.9215031 ln E) x BR / E (4)

Where E = activation energy, B = heating rate, A = frequency factor, and α = fraction of the sample decomposed at time't' [18].

A computer program has been written for the calculation of kinetic data by using Coats-Redfern equation, in which data can be cycled for any value of n (order of reaction) until the best fit is obtained (by least mean squares) . The kinetic data are also analyzed by two dimensional diffusion equation and by three dimensional phase boundary reaction (Table 1). Plots for typical experiments are shown for non-

isothermal TGA, EGA and DTA of $FeC_2O_4.2H_2O$, $BaC_2O_4.0.6H_2O$ and binary mechanical mixture of $BaC_2O_4.0.6H_2O$ and $FeC_2O_4.2H_2O$ in mole ratio (1:1) in figure1, figure 2 and figure 3.

Table-1 Kinetic equations examined in this work

Reaction model	G (α)	Symbol
One dimensional diffusion	α^2	D_1
Two dimensional diffusion	(1-α) ln (1- α) + α	D_2
Jander equation, Three dimensional diffusion	$[1- (1-\alpha)^{1/3}]^2$	D_3
Ginling Braunshtein equation, Three dimensional diffusion	$[1- 2\alpha / 3] -(1-\alpha)^{2/3}$	D_4
Two dimentional phase boundary reaction.	$[1 – (1-\alpha)^{1/2}]$	R_2
Three dimensional phase boundary reaction.	$[1 – (1-\alpha)^{1/3}]$	R_3
First order kinetics, Mampel unimolecular law, Random nucleation.	[- ln (1-α)]	F_1
Random nucleation: Avrami equation.	$[– \ln (1-\alpha)]^{1/2}$	A_2
Random nucleation: Erofeev equation	$[– \ln (1-\alpha)]^{1/3}$	A_3
Exponential law	ln α	E_1

3. RESULT AND DISCUSSION

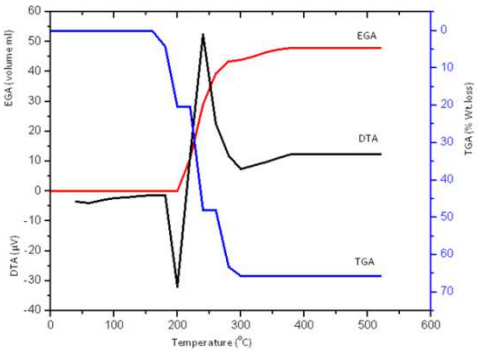

Fig.1: DTA-TGA-EGA curves of $FeC_2O_4.2H_2O$ in air at heating rate of 4^0C min^{-1}

TGA, EGA and DTA the temperature range selected is R.T to 1000 °C. TGA, EGA and DTA of $FeC_2O_4.2H_2O$ is shown in fig.1. The TGA shows two distinct steps. The first step observed in the temperature range 180 ^{0}C to 200 ^{0}C and is accompanied with 20.03% mass loss [19]. This is attributed to the water loss, equivalent to two water molecules (calculated mass loss 20.01%). The second step occurs in the temperature range 240 ^{0}C to 300 ^{0}C showing weight loss 45.19% against the calculated mass loss 45.18% [20]. This mass loss corresponds to the complete conversion of FeC_2O_4 to Fe_2O_3. The anhydrous mixture is used for EGA study. EGA shows the theoretical volume, for decomposition at N.T.P condition to be 47.55 ml against the observed volume at N.T.P is 48.00 ml which results in decomposition of FeC_2O_4 to Fe_2O_3 at 380 ^{0}C. The DTA shows sharp 'Endo' pick at 200 ^{0}C for loss of water of crystallization and second sharp 'Exo' peak at 250 ^{0}C for decomposition of FeC_2O_4.

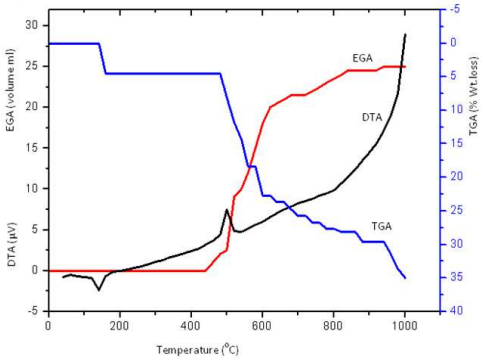

Fig.2: DTA-TGA-EGA curves of $BaC_2O_4.0.6H_2O$ in air at heating rate of 4^0C min^{-1}

The $BaC_2O_4.0.6H_2O$ is decomposed within three steps (Fig2). The first step observed at 160 ^{0}C to 180 ^{0}C and is accompanied by 4.54% mass loss [21]. This is attributed to the 0.6 water molecule (calculated mass loss 4.57%). The second step shows decomposition to $BaCO_3$ at 450 ^{0}C to 560 ^{0}C accompanied by 12.59% mass loss while calculated mass loss is 12.42% [22]. The third step shows decomposition of $BaCO_3$ to 80% BaO in the temperature range 600 ^{0}C to 1000 ^{0}C[23] accompanied by 17.83% mass loss while calculated mass loss is 17.83%. The pure individual barium (II) oxalate shows complete decomposition at 1385 °C[24] this is due to CO formed in the temperature range 480 °C – 500 °C is again recombine to form $BaCO_3$, it may be due to small crystallite size of $BaCO_3$ or due to formation of defects in the crystallite. EGA study shows the volume for decomposition of BaC_2O_4 by calculation at N.T.P condition is 24.56 ml and observed volume at N.T.P is 25.00 ml, which results in decomposition of BaC_2O_4 to $BaCO_3$ up to 1000 ^{0}C. The DTA shows 'Endo' peak at 180 ^{0}C for water loss and sharp 'Exo' peak at 500 ^{0}C indicating starting of decomposition of BaC_2O_4 to $BaCO_3$.

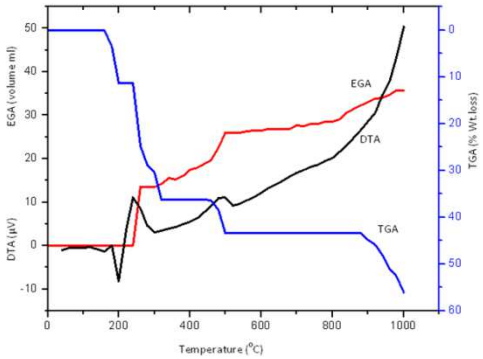

Fig.3: DTA-TGA-EGA curves of $BaC_2O_4.0.6H_2O$ and $FeC_2O_4.2H_2O$ in mole ratio (1:1) in air at heating rate of 4^{0}C min^{-1}

In the mixture of $BaC_2O_4.0.6H_2O$ and $FeC_2O_4.2H_2O$ in mole ratio (1:1) (Fig3) shows four distinct steps for mass loss. The complete dehydration observed in the temperature range 180 ^{0}C - 200 ^{0}C and is accompanied by 11.27% mass loss [25]. This is attributed to the 2.6 water molecules (calculated mass loss 11.25%). Anhydrous mixture is thermally unstable and shows distinct three consecutive mass loss steps. In the second step the decomposition of FeC_2O_4 to Fe_2O_3 in the temperature range 260 ^{0}C to 320 ^{0}C is observed with mass loss 24.93% [26] and calculated mass loss is 24.95%. The third step is the decomposition of BaC_2O_4 to $BaCO_3$ in temperature range 480 ^{0}C to 500 ^{0}C [27] where observed mass loss is 8.38% and calculated mass loss is 8.41% Equivalent to 1/10 of formation of BaO. The X-ray study of end product of binary mixture of $BaC_2O_4.0.6H_2O$ and $FeC_2O_4.2H_2O$ in mole ratio (1:1) taken at 500 ^{0}C support the formation of 90% $BaCO_3$ and 10% BaO. This occurs at lower temperature than the decomposition of pure BaC_2O_4 where there is no BaO formation observed in this temperature range. The mixture shows complete conversion of $BaCO_3$ to BaO in temperature range 900 ^{0}C to 1000 ^{0}C and is supported by X-ray taken at 900 ^{0}C, where formation of 100% BaO. While in pure BaC_2O_4 no BaO formation is reported in this temperature range [28]. Last step shows the decomposition of $BaCO_3$ to BaO in temperature range 900 ^{0}C to1000 ^{0}C where observed mass loss is 11.27% and calculated mass loss is 11.23% [29] for complete conversion of $BaCO_3$ to BaO, actually in the pure BaC_2O_4 system the complete conversion of $BaCO_3$ to BaO takes place at temperature [30] greater than 1000 ^{0}C.

But the presence of Fe_2O_3 which acts as catalyst, the decomposition of $BaCO_3$ to BaO occurs at lower temperature [31-32]. EGA study shows the volume for decomposition at N.T.P condition is 35.95 ml and observed volume at N.T.P is 35.75 ml, which results in decomposition of BaC_2O_4 and FeC_2O_4 (1:1) mole ratio mixture to Fe_2O_3 and $BaCO_3$ at 1000 ^{0}C. When the binary mixture of Ferrous (II) oxalate and barium (II) oxalate in the mole ratio 1:1 is heated dynamically as the decomposition temperature of Ferrous (II) oxalate is 240 °C. It decomposes completely at 320 °C forming Fe_2O_3 and that remain with barium (II) oxalate which starts decomposition at 480 °C. In case of thermal decomposition of individual barium (II) oxalate the decomposition complete at 1385 °C are higher and are found to be lower in presence of Fe_2O_3 in our mixture.

3.1 X-ray Diffraction

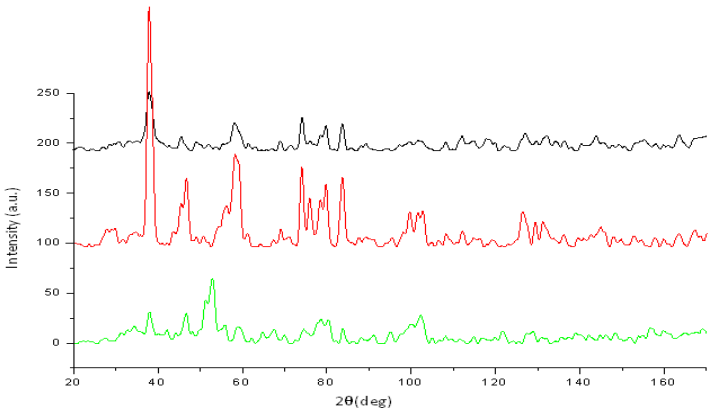

Fig.4: X-ray powder diffractograms of solid $BaC_2O_4.0.6H_2O$ and $FeC_2O_4.2H_2O$ (1:1) mole ratio mixture obtained at (a) 500^{0}C, (b) 700^{0}C and (c) 900^{0}C

The XRD diffraction pattern of the initial mixture matched the standard data compiled in the JCPDS data. The sample of $FeC_2O_4.2H_2O$ and $BaC_2O_4.0.6H_2O$ in mole ratio (1:1) is heated in an open air at 500^{0}C, 700^{0}C and 900^{0}C with a linear heating rate of 4-5 ^{0}C/ min and their XRD pattern is recorded in 2θ range of 20-180^0. The XRD pattern of the sample at 500^{0}C, 700^{0}C and 900^{0}C showed the formation of orthorombic $BaFe_2O_4$ (JCPDS no.772337) and $BaCO_3$ (JCPDS no.85-0720)[33]. The orthorombic $BaCO_3$ further decomposed to BaO at 1000^{0}C. The decomposition reaction of $BaC_2O_4.0.6H_2O$ and $FeC_2O_4.2H_2O$ in mole ratio (1:1) for TGA is shown below. In our study the formation of $BaFe_2O_4$ from temperature 500 °C to 900 °C and is confirmed by XRD. This is found to be reported to form such type of phase by other methods.

Step: I 180 ^{0}C to 200 ^{0}C

$BaC_2O_4.0.6H_2O$: $FeC_2O_4.H_2O$ $\longrightarrow$ BaC_2O_4: FeC_2O_4 + 2.6 H_2O

(Observed Wt. loss = 11.27%), (Calculated Wt. loss = 11.25%)

Step: II

$$BaC_2O_4{:}\ 2FeC_2O_4 \xrightarrow{260\ ^0C \text{ to } 320\ ^0C} BaC_2O_4{:}Fe_2O_3 + 3CO\uparrow + CO_2\uparrow$$

(Observed Wt. loss = 24.93%), (Calculated Wt. loss = 24.95 %)

Step: III

$$BaC_2O_4{:}Fe_2O_3 \xrightarrow{480\ ^0C \text{ to } 500\ ^0C} Fe_2O_3 + 9/10BaCO_3 + 1/10BaO + CO\uparrow + 1/10CO_2\uparrow$$

(Observed Wt. loss = 8.38%), (Calculated Wt. loss = 8.41%)

Step: IV

$$9/10BaCO_3{:}1/10BaO{:}Fe_2O_3 \xrightarrow{900\ ^0C \text{ to } 1000\ ^0C} Fe_2O_3 + BaO + 9/10CO_2\uparrow$$

(Observed Wt. loss = 11.27%), (Calculated Wt. loss = 11.23%)

Five different temperatures 550 ^{0}C, 500 ^{0}C, 450 ^{0}C, 400 ^{0}C, 350 ^{0}C, 300 ^{0}C and 250 ^{0}C were selected for conducting isothermal kinetic studies of TGA and 550 ^{0}C, 500 ^{0}C, 450 ^{0}C, 400 ^{0}C, 350 ^{0}C, 300 ^{0}C for EGA techniques. TGA and EGA (Fig.5 and 6) shows the variation of degree of decomposition (α) of $BaC_2O_4.0.6H_2O$ and $FeC_2O_4.2H_2O$ (1:1) mole ratio mixture to Fe_2O_3, $BaCO_3$ and BaO with time at different isothermal conditions[34]. The data obtained from isothermal method using TGA and EGA techniques are plotted as degree of decomposition (α) as a function of time ($t/t_{0.5}$) (Fig.7 and 8)[35]. These sigmoid shaped curves are characteristics of a mechanism by which the decomposition occurs at the interface between the product and un-decomposed reactant.

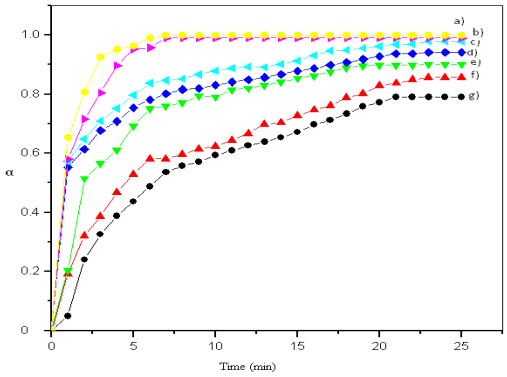

Fig.5 Isothermal decomposition curves (TGA) for $BaC_2O_4.0.6H_2O$ and $FeC_2O_4.2H_2O$ (1:1) mole ratio mixture at a) 250 ^{0}C, b) 300 ^{0}C, c) 3500 ^{0}C, d) 400 ^{0}C, e) 450 ^{0}C, f) 500 ^{0}C and g) 550 ^{0}C

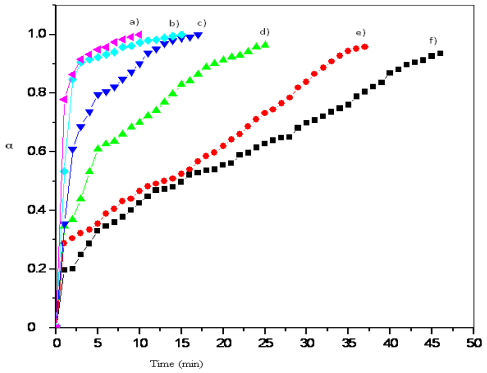

Fig.6 Isothermal decomposition curves (EGA) for $BaC_2O_4.0.6H_2O$ and $FeC_2O_4.2H_2O$ (1:1) mole ratio mixture at a) 300^{0}C, b) 350 ^{0} C c) 400 ^{0}C, d) 450 ^{0}C, e) 500 ^{0}C and f) 550 ^{0}C

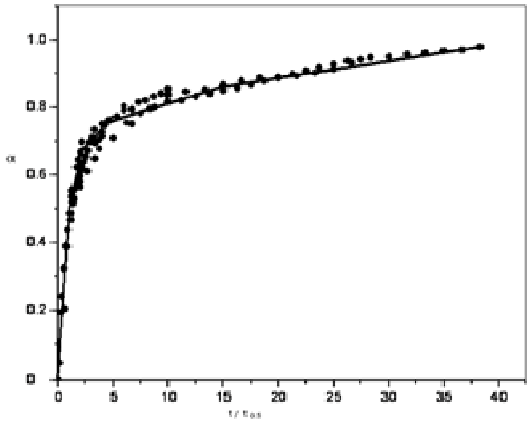

Fig.7: α Vs. t / $t_{0.5}$ plots of TGA for isothermal decomposition of $BaC_2O_4.0.6H_2O$ and $FeC_2O_4.2H_2O$ (1:1) mole ratio

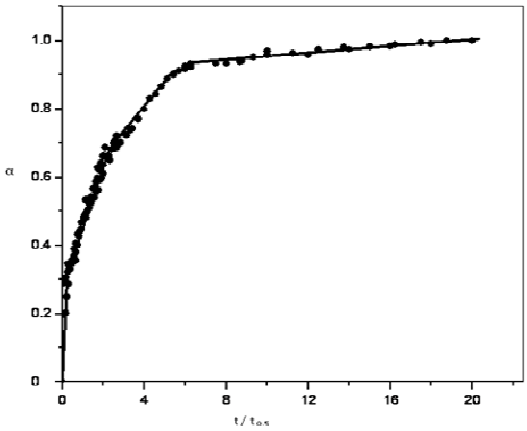

Fig.8 α Vs. t / $t_{0.5}$ plots of EGA for isothermal decomposition of $BaC_2O_4.0.6H_2O$ and $FeC_2O_4.2H_2O$ (1:1) mole ratio

The kinetic parameters evaluated by TGA using non-mechanistic equations are given in table2. The Ea of decomposition process using non-isothermal TGA and EGA method [36] is found to be 15.07 KJ/mole and 16.57 KJ/mole by plotting ln k Vs. $T^{-1}.10^3/K^{-1}$ respectively (Fig.9 and 10) [37]. The order (n) of decomposition reaction of binary mixture using TGA and EGA is 0.70 and 2.20 respectively[38].

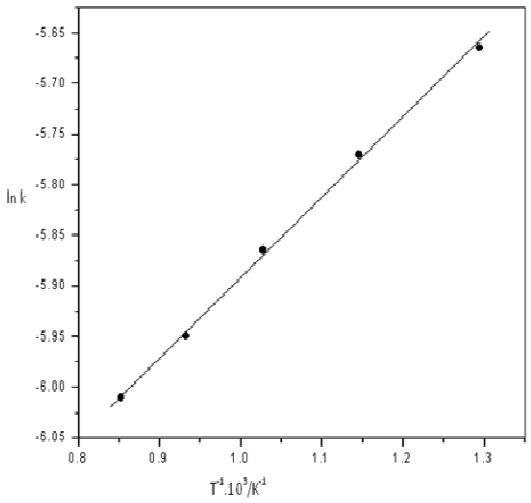

Fig.9 Arrhenius plot: of ln k Vs. $T^{-1}.10^3/K^{-1}$ of dynamic TGA of $BaC_2O_4.0.6H_2O$ and $FeC_2O_4.2H_2O$ (1:1) mole ratio

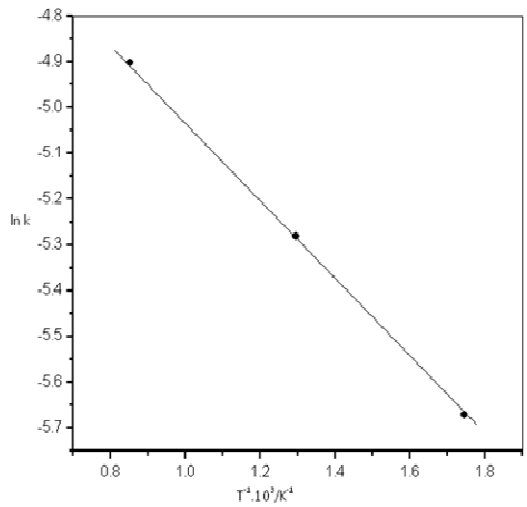

Fig.10: Arrhenius plot: of ln k Vs. $T^{-1}.10^3/K^{-1}$ of dynamic EGA of $BaC_2O_4.0.6H_2O$ and $FeC_2O_4.2H_2O$ (1:1) mole ratio

Isothermal TGA method using three dimensional diffusion is 15.36 KJ/mole and Avrami equation is 13.48 KJ/mole by plotting log $[1- (1-\alpha)^{1/3}]^2$ Vs $T^{-1}.10^3/K^{-1}$ and log $[- \ln (1-\alpha)]^{1/2}$ Vs. $T^{-1}.10^3/K^{-1}$ (fig.11 and 12) respectively. The EGA method using two dimentional phase boundary reaction is 15.36 KJ/mole and Avrami equation is 13.48 KJ/mole by plotting log $[1 - (1-\alpha)^{1/2}]$ Vs $T^{-1}.10^3/K^{-1}$ and log $[- \ln (1-\alpha)]^{1/2}$ Vs. $T^{-1}.10^3/K^{-1}$ (fig.13 and 14) respectively. In EGA technique the decomposition temperature and Ea (activation energy) is high due to closed system. The correlation coefficient (r) for TGA and EGA are in the range 0.9983 - 0.9999, indicating nearly perfect fits[39].

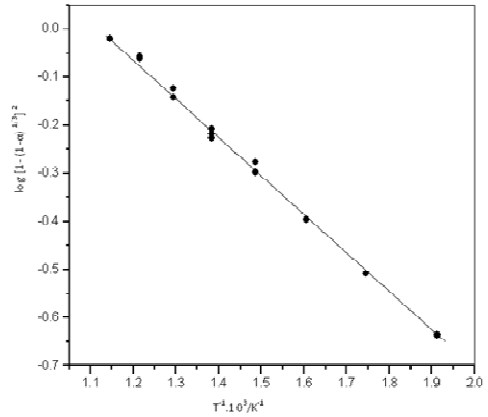

Fig.11 Arrhenius plot for TGA of log $[1- (1-\alpha)^{1/3}]^2$ Vs $T^{-1}.10^3/K^{-1}$ for decomposition of $BaC_2O_4.0.6H_2O$ and $FeC_2O_4.2H_2O$ (1:1) mole ratio

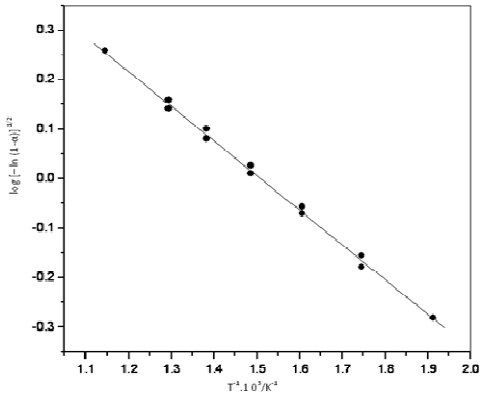

Fig.12 Arrhenius plot for TGA of log $[- \ln (1-\alpha)]^{1/2}$ Vs $T^{-1}.10^3/K^{-1}$ for decomposition of $BaC_2O_4.0.6H_2O$ and $FeC_2O_4.2H_2O$ (1:1) mole ratio

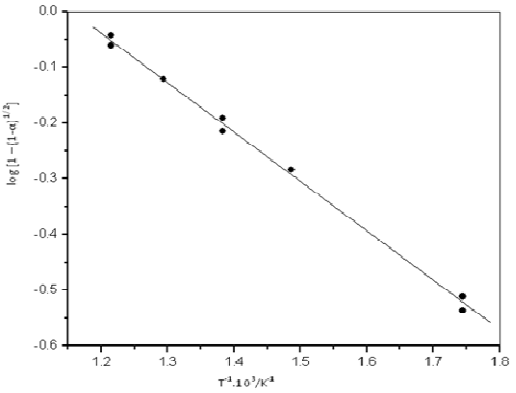

Fig.13 Arrhenius plot for EGA of log $[1 - (1-\alpha)^{1/2}]$ Vs $T^{-1}.10^3/K^{-1}$ for decomposition of $BaC_2O_4.0.6H_2O$ and $FeC_2O_4.2H_2O$ (1:1) mole ratio

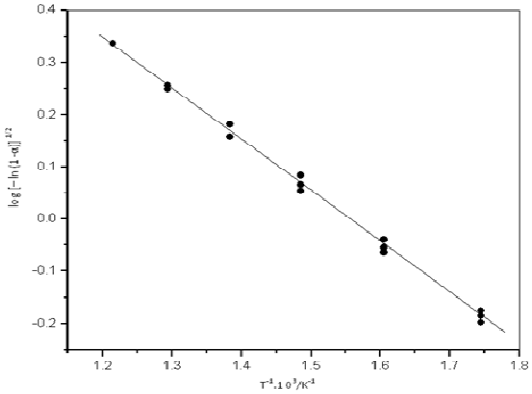

Fig.14 Arrhenius plot for EGA of log $[- \ln (1-\alpha)]^{1/2}$ Vs $T^{-1}.10^3/K^{-1}$ for decomposition of $BaC_2O_4.0.6H_2O$ and $FeC_2O_4.2H_2O$ (1:1) mole ratio

The decomposition of binary mixture using TGA can be found out by plotting $[1- (1-\alpha)^{1/3}]^2$ Vs. time (min) and $[-\ln (1-\alpha)]^{1/2}$ Vs. time (min) (Fig.15 and 16) and obey three dimensional diffusion followed by random nucleation (Avrami equation). While using EGA decomposition can be found out by plotting $[1 - (1-\alpha)^{1/2}]$ Vs. time (min) and $[-\ln (1-\alpha)]^{1/2}$ Vs. time (min) (Fig.17 and 18) and obey two dimentional phase boundary reaction followed by random nucleation (Avrami equation).

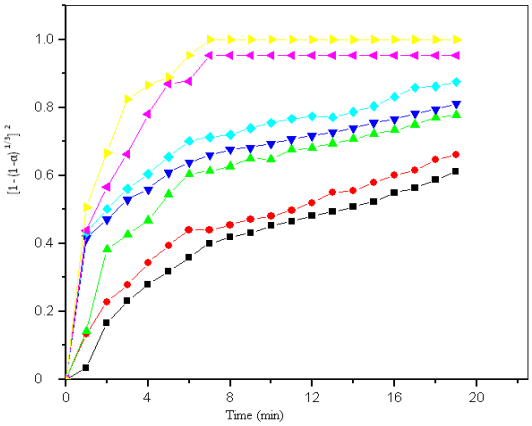

Fig.15 (TGA) plot of $[1- (1-\alpha)^{1/3}]^2$ Vs time of decomposition of $BaC_2O_4.0.6H_2O$ and $FeC_2O_4.2H_2O$ (1:1) mole ratio

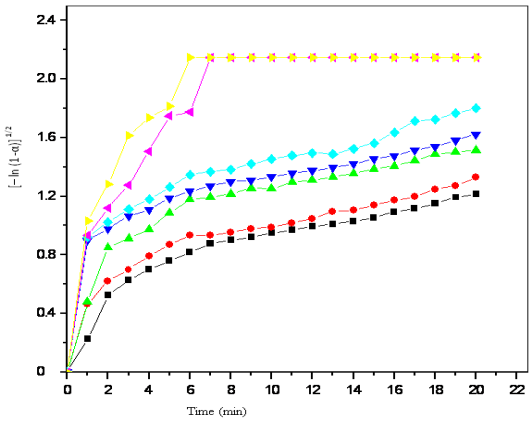

Fig.16 (TGA) plot of $[-\ln (1-\alpha)]^{1/2}$ Vs time of decomposition of $BaC_2O_4.0.6H_2O$ $FeC_2O_4.2H_2O$ (1:1) mole ratio

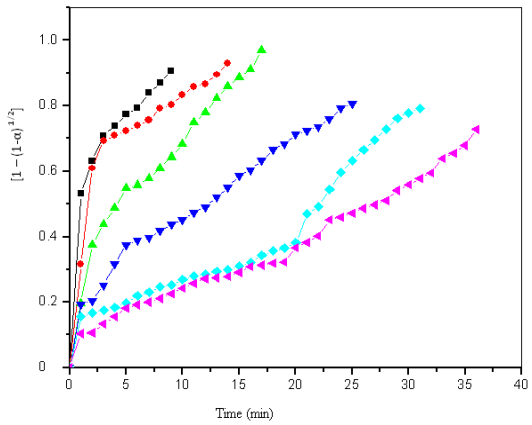

Fig.17 (EGA) plot of $[1 - (1-\alpha)^{1/2}]$ Vs time of decomposition of $BaC_2O_4.0.6H_2O$ and $FeC_2O_4.2H_2O$ (1:1) mole ratio

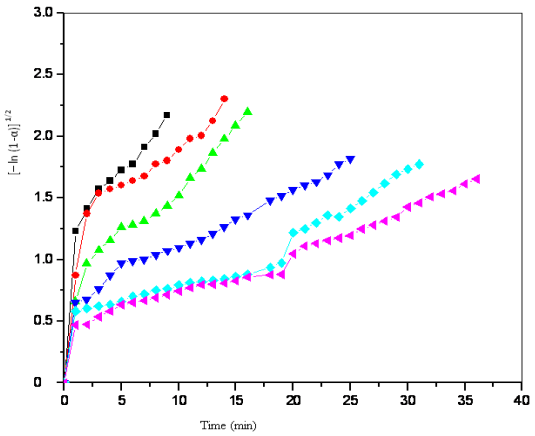

Fig.18: (EGA) plot of $[-\ln (1-\alpha)]$ ½ Vs time of decomposition of $BaC_2O_4.0.6H_2O$ $FeC_2O_4.2H_2O$ (1:1) mole ratio

Table-2 Activation parameters of the isothermal and dynamic decomposition in air of $BaC_2O_4.0.6H_2O$ and $FeC_2O_4.2H_2O$ (1:1) mole ratio mixture by TGA and EGA method

Method of analysis	Ea (activation energy) in KJ/mole.	A,(frequency factor)	r, (correlation coefficient)	n, Order of reaction
Non-isothermal TGA	15.07	$4.19x10^5$	0.9992	0.70
Isothermal TGA by three dimensional diffusion	15.36	$1.32x10^3$	0.9983	0.70
Isothermal TGA by Avrami equation	13.48	$1.52x10^3$	0.9983	0.70
Non-isothermal EGA	16.57	$3.38x10^4$	0.9999	2.20
Isothermal EGA by two dimentional phase boundary reaction	16.91	$1.46x10^3$	0.9983	2.20
Isothermal EGA by Avrami equation	18.48	$2.41x10^3$	0.9982	2.20

Proofs: Data of above graphs.
Fig1.

Temperature (^{0}C)	EGA (Volume in ml)	DTA (µV)	TGA (% Wt. loss)
0	0	--	0
40	0	-3.53	0
60	0	-4.05	0
80	0	-3.08	0
100	0	-2.4	0
120	0	-2.08	0
140	0	-1.54	0
160	0	-1.37	0
180	0	-1.31	4.3222
200	0	-31.92	20.4322
220	11	11.78	20.4322
240	29	52.48	48.1335
260	39.5	22.64	48.1335
280	43.5	12.04	63.2612
300	44	7.38	65.6188
320	45	8.55	65.6188
340	46.5	9.77	65.6188
360	47.5	11.07	65.6188
380	48	12.44	65.6188
400	48	12.44	65.6188
420	48	12.44	65.6188
440	48	12.44	65.6188
460	48	12.44	65.6188
500	48	12.44	65.6188
520	48	12.44	65.6188

Fig2.

Temperature (^{0}C)	EGA (Volume in ml)	DTA (µV)	TGA (% Wt. loss)
0	0	--	0
40	0	-0.75167	0
60	0	-0.525	0
80	0	-0.7	0
100	0	-0.755	0
120	0	-0.83167	0
140	0	-2.38833	0
160	0	-0.695	4.5454
180	0	-0.12667	4.5454
200	0	-0.02167	4.5454
220	0	0.20167	4.5454
240	0	0.36333	4.5454
260	0	0.57167	4.5454
280	0	0.82167	4.5454
300	0	1.075	4.5454
320	0	1.33667	4.5454
340	0	1.67333	4.5454
360	0	1.90167	4.5454
380	0	2.15333	4.5454
400	0	2.4	4.5454
420	0	2.74333	4.5454
440	0	3.15333	4.5454
460	1	3.61667	4.5454
480	2	4.425	4.5454
500	2.5	7.52167	8.0419
520	9	4.89667	11.7132
540	10	4.76333	14.3356
560	12	5.11667	18.3566
580	15	5.62333	18.3566
600	18	6.05167	22.7272
620	20	6.53667	22.7272
640	20.5	7.035	23.6013
660	21	7.49167	23.6013
680	21.5	7.84167	24.8251
700	21.5	8.24167	25.6993
720	21.5	8.51667	25.6993
740	22	8.79167	26.7482
760	22.5	9.19667	26.7482
780	23	9.49333	27.6223
800	23.5	9.82333	27.6223
820	24	10.67833	28.1468
840	24.5	11.49	28.1468
860	24.5	12.45	28.1468
880	24.5	13.52667	29.5454
900	24.5	14.495	29.5454
920	24.5	15.61333	29.5454
940	25	17.165	29.5454
960	25	18.89167	31.2937
980	25	21.68167	33.5664
1000	25	28.92167	34.965

Fig3.

Temperature (^{0}C)	EGA (Volume in ml)	DTA (µV)	TGA (% Wt. loss)
0	0	--	0
40	0	-0.94667	0
60	0	-0.45333	0
80	0	-0.50667	0
100	0	-0.39667	0
120	0	-0.31333	0
140	0	-0.87667	0
160	0	-1.41333	0
180	0	0.00667	3.61
200	0	-8.19333	11.27
220	0	3.52	11.27
240	0	11.16667	11.27
260	13.5	8.52667	24.85
280	13.5	4.70333	28.75
300	13.5	3.15667	30.49
320	14.25	3.42	36.27
340	15.5	3.92	36.27
360	15.25	4.30333	36.27
380	16	4.95667	36.27
400	17.5	5.56	36.27
420	18	6.39333	36.27
440	18.75	7.70333	36.27
460	19.75	9.16333	36.41
480	22.5	11.03333	38.5
500	26	11.14333	43.35
520	26	9.22333	43.35
540	26	9.63667	43.35
560	26.25	10.4	43.35
580	26.5	11.18	43.35
600	26.5	12.10667	43.35
620	26.75	13.16667	43.35
640	26.75	14.04333	43.35
660	26.75	14.92333	43.35
680	26.75	15.93333	43.35
700	27.75	16.69667	43.35
720	27.5	17.42	43.35
740	28	18.11	43.35
760	28	18.61667	43.35
780	28.5	19.46667	43.35
800	28.5	20.18	43.35
820	29	21.62	43.35
840	30.5	23.03667	43.35
860	31.5	24.72333	43.35
880	32.25	26.56333	43.35
900	33	28.6	44.79
920	33.75	30.50667	45.95
940	34	34.43333	47.97
960	34.75	37.68667	51.01
980	35.75	43.15667	52.6
1000	35.75	50.29333	56.06

Fig5.

X-axis values of Time (min)	Y-axis values of α, at 250 ^{0}C	Y-axis values of α, at 300 ^{0}C	Y-axis values of α, at 350 ^{0}C	Y-axis values of α, at 400 ^{0}C	Y-axis values of α, at 450 ^{0}C	Y-axis values of α, at 500 ^{0}C	Y-axis values of α, at 550 ^{0}C
0	0	0	0	0	0	0	0
1	0.049	0.193	0.204	0.553	0.572	0.58	0.653
2	0.24	0.32	0.515	0.615	0.648	0.715	0.807
3	0.326	0.387	0.565	0.677	0.709	0.804	0.926
4	0.388	0.467	0.612	0.708	0.751	0.897	0.951
5	0.437	0.529	0.693	0.755	0.797	0.953	0.963
6	0.487	0.581	0.751	0.782	0.837	0.957	0.99
7	0.536	0.581	0.76	0.801	0.846	0.99	1
8	0.557	0.597	0.772	0.816	0.852	0.99	1
9	0.571	0.615	0.793	0.82	0.867	0.99	1
10	0.594	0.624	0.791	0.831	0.879	0.99	1
11	0.609	0.644	0.815	0.841	0.888	0.99	1
12	0.627	0.667	0.82	0.849	0.893	0.99	1
13	0.639	0.699	0.831	0.857	0.891	0.99	1
14	0.654	0.704	0.841	0.867	0.902	0.99	1
15	0.671	0.728	0.854	0.879	0.913	0.99	1
16	0.697	0.747	0.862	0.887	0.931	0.99	1
17	0.712	0.761	0.875	0.899	0.947	0.99	1
18	0.734	0.789	0.89	0.907	0.949	0.99	1
19	0.759	0.802	0.895	0.918	0.956	0.99	1
20	0.772	0.829	0.899	0.928	0.961	0.99	1
21	0.79	0.837	0.899	0.937	0.968	0.99	1
22	0.791	0.849	0.899	0.937	0.97	0.99	1
23	0.791	0.857	0.901	0.942	0.979	0.99	1
24	0.791	0.857	0.901	0.942	0.979	0.99	1
25	0.791	0.857	0.901	0.942	0.979	0.99	1

Fig6.

X-axis values of Time (min)	Y-axis values of α, at 300 ^{0}C	Y-axis values of α, at 350 ^{0}C	Y-axis values of α, at 400 ^{0}C	Y-axis values of α, at 450 ^{0}C	Y-axis values of α, at 500 ^{0}C	Y-axis values of α, at 550 ^{0}C
0	0	0	0	0	0	0
1	0.197	0.288	0.347	0.355	0.533	0.7796
2	0.201	0.305	0.368	0.61	0.847	0.864
3	0.249	0.322	0.44	0.686	0.906	0.915
4	0.287	0.334	0.533	0.737	0.915	0.932
5	0.331	0.355	0.61	0.796	0.923	0.949
6	0.347	0.389	0.627	0.805	0.932	0.957
7	0.36	0.406	0.635	0.822	0.94	0.974
8	0.378	0.432	0.661	0.848	0.957	0.983
9	0.401	0.44	0.684	0.873	0.961	0.991
10	0.425	0.466	0.7	0.9	0.972	1
11	0.448	0.483	0.723	0.937	0.98	--
12	0.469	0.491	0.741	0.951	0.982	--
13	0.473	0.5	0.77	0.969	0.989	--
14	0.48	0.508	0.798	0.98	0.995	--
15	0.497	0.525	0.829	0.987	1	--
16	0.521	0.54	0.843	0.992	--	--
17	0.529	0.567	0.865	0.999	--	--
18	0.537	0.585	0.888	--	--	--
19	0.54	0.597	0.9	--	--	--
20	0.555	0.62	0.912	--	--	--
21	0.561	0.642	0.924	--	--	--
22	0.589	0.66	0.93	--	--	--
23	0.597	0.687	0.942	--	--	--
24	0.615	0.711	0.957	--	--	--
25	0.628	0.732	0.963	--	--	--
26	0.639	0.744	--	--	--	--
27	0.648	0.765	--	--	--	--
28	0.65	0.784	--	--	--	--
29	0.681	0.819	--	--	--	--
30	0.699	0.838	--	--	--	--
31	0.708	0.865	--	--	--	--
32	0.721	0.887	--	--	--	--
33	0.736	0.908	--	--	--	--
34	0.748	0.927	--	--	--	--
35	0.76	0.943	--	--	--	--
36	0.789	0.951	--	--	--	--
37	0.805	0.957	--	--	--	--
38	0.822	--	--	--	--	--
39	0.836	--	--	--	--	--
40	0.869	--	--	--	--	--
41	0.881	--	--	--	--	--
42	0.897	--	--	--	--	--
43	0.905	--	--	--	--	--
44	0.912	--	--	--	--	--
45	0.926	--	--	--	--	--
46	0.935	--	--	--	--	--

Fig.7

X-axis values of $t / t_{0.5}$	Y-axis values of α	X-axis values of $t / t_{0.5}$	Y-axis values of α
0	0	6.666	0.751
0.1818	0.049	6.25	0.755
0.2857	0.193	4.666	0.76
0.666	0.204	4.5714	0.761
0.3636	0.24	5.333	0.772
0.5714	0.32	7.5	0.782
0.5454	0.326	6	0.791
0.8571	0.387	6.666	0.793
0.7272	0.388	8.3333	0.797
0.909	0.437	8.75	0.801
1.1428	0.467	6	0.804
1.0909	0.487	7.333	0.815
1.333	0.515	10	0.816
1.4285	0.529	8	0.82
1.2727	0.536	11.25	0.82
1.25	0.553	8.666	0.831
1.4545	0.557	12.5	0.831
2	0.565	10	0.837
1.6363	0.571	9.333	0.841
1.666	0.572	13.75	0.841
2	0.58	11.666	0.846
1.7142	0.581	15	0.849
1.8181	0.594	13.333	0.852
2	0.597	10	0.854
2	0.609	16.25	0.857
2.666	0.612	17.5	0.867
2.2857	0.615	15	0.867
2.5	0.615	18.75	0.879
1.6363	0.624	16.666	0.879
2.1818	0.627	20	0.887
2.3636	0.639	18.333	0.888
1.8181	0.644	20	0.891
3.333	0.648	21.666	0.893
2.5	0.653	21.25	0.899
2.5454	0.654	23.333	0.902
2	0.667	22.5	0.907
2.7272	0.671	23.75	0.918
3.75	0.677	--	0.902
3.333	0.693	25	0.913
2.909	0.697	25	0.928
2.1818	0.699	26.666	0.931
3.7142	0.704	26.25	0.937
5	0.708	27.5	0.942
5	0.709	28.333	0.947
3.0909	0.712	30	0.949
4	0.715	31.666	0.956
4	0.728	33.333	0.961
3.2727	0.734	35	0.968
4.2857	0.747	36.666	0.97
4	0.751	38.333	0.979

Fig. 8

X-axis values of $t / t_{0.5}$	Y-axis values of α	X-axis values of $t / t_{0.5}$	Y-axis values of α
0	0	2	0.66
0.0833	0.197	2.095	0.687
0.166	0.201	0.857	0.44
0.095	0.288	1.142	0.533
0.25	0.249	1.714	0.627
0.333	0.287	2	0.635
0.19	0.305	2.285	0.661
0.285	0.322	2.5714	0.684
0.416	0.331	2.857	0.7
0.38	0.334	3.142	0.723
0.5	0.347	3.428	0.741
0.285	0.347	3.714	0.77
0.666	0.355	4	0.798
0.476	0.355	4.285	0.829
0.583	0.36	4.571	0.843
0.571	0.368	4.857	0.865
0.666	0.378	5.142	0.888
0.571	0.389	5.428	0.9
0.75	0.401	5.714	0.912
0.833	0.425	6	0.924
0.916	0.448	6.285	0.93
1	0.469	2	0.61
1.083	0.473	2.666	0.686
1.166	0.48	3.333	0.737
1.25	0.497	8.666	0.937
1.333	0.521	9.333	0.951
1.416	0.529	10	0.969
1.5	0.537	10.666	0.98
1.583	0.54	11.333	0.987
1.666	0.555	12	0.992
1.75	0.561	12.666	0.999
1.833	0.589	1.25	0.533
1.916	0.597	6.25	0.923
2.333	0.65	7.5	0.932
2.416	0.681	8.75	0.94
2.5	0.699	10	0.957
2.583	0.708	11.25	0.961
2.666	0.721	12.5	0.972
0.666	0.406	13.75	0.98
0.761	0.432	15	0.982
0.857	0.44	16.25	0.989
0.952	0.466	17.5	0.995
1.047	0.483	18.75	1
1.142	0.491	6	0.915
1.238	0.5	8	0.932
1.333	0.508	12	0.957
1.428	0.525	14	0.974
1.428	0.54	16	0.983
1.523	0.567	18	0.991
1.619	0.585	20	1
1.714	0.597		
1.809	0.62		
1.904	0.642		

Fig9.

X- axis values of $T^{-1}.10^3/K^{-1}$	Y- axis values of ln k
0.85251	-6.01056
0.93197	-5.94979
1.02775	-5.86482
1.14548	-5.77062
1.29366	-5.66495

Fig10.

X- axis values of $T^{-1}.10^3/K^{-1}$	Y- axis values of ln k
0.85251	-4.90207
1.29366	-5.28162
1.7452	-5.67194

Fig11.

X- axis values of $T^{-1}.10^3/K^{-1}$	Y- axis values of $\log [1- (1-\alpha)^{1/3}]^2$
1.91205	-0.63588
1.7452	-0.50846
1.60514	-0.3963
1.48588	-0.29812
1.48588	-0.27635
1.38312	-0.22721
1.38312	-0.21881
1.38312	-0.20742
1.29366	-0.14178
1.29366	-0.12417
1.21507	-0.0606
1.21507	-0.05687
1.14548	-0.02064

Fig12.

X- axis values of $T^{-1}.10^3/K^{-1}$	Y- axis values of $\log [- \ln (1-\alpha)]^{1/2}$
1.91205	-0.28078
1.7452	-0.17825
1.7452	-0.15517
1.60514	-0.07025
1.60514	-0.05675
1.48588	0.01056
1.48588	0.02656
1.38312	0.08105
1.38312	0.10132
1.29366	0.14135
1.29366	0.15981
1.14548	0.25905

Fig13.

X- axis values of $T^{-1}.10^3/K^{-1}$	Y- axis values of $\log [1 - (1-\alpha)^{1/2}]$
1.21507	-0.06067
1.21507	-0.04329
1.29366	-0.12202
1.38312	-0.21458
1.38312	-0.19136
1.48588	-0.28365
1.7452	-0.53644
1.7452	-0.51159

Fig14.

X- axis values of $T^{-1}.10^3/K^{-1}$	Y- axis values of $\log [- \ln (1-\alpha)]^{1/2}$
1.21507	0.33653
1.29366	0.24892
1.29366	0.25555
1.38312	0.15731
1.38312	0.18111
1.48588	0.05424
1.48588	0.06532
1.48588	0.08361
1.60514	-0.06409
1.60514	-0.05492
1.60514	-0.03863
1.7452	-0.1979
1.7452	-0.1852
1.7452	-0.17519

Fig15.

X-axis values of Time (min)	Y-axis values of α, at 250 ^{0}C	Y-axis values of α, at 300 ^{0}C	Y-axis values of α, at 350 ^{0}C	Y-axis values of α, at 400 ^{0}C	Y-axis values of α, at 450 ^{0}C	Y-axis values of α, at 500 ^{0}C	Y-axis values of α, at 550 ^{0}C
0	0	0	0	0	0	0	0
1	0.0329	0.1332	0.1411	0.4154	0.4321	0.4392	0.5062
2	0.1672	0.2267	0.3827	0.4708	0.5015	0.5669	0.666
3	0.2313	0.2784	0.4259	0.5292	0.5609	0.6626	0.8237
4	0.2792	0.3426	0.468	0.5599	0.6042	0.7803	0.8661
5	0.3182	0.3946	0.5449	0.6085	0.6546	0.8698	0.889
6	0.3592	0.4401	0.6042	0.6378	0.7016	0.8773	0.9536
7	0.4007	0.4401	0.6138	0.6591	0.7127	0.9536	1
8	0.4189	0.4544	0.6268	0.6765	0.7202	0.9536	1
9	0.4312	0.4708	0.6501	0.6812	0.7394	0.9536	1
10	0.4517	0.4791	0.6478	0.6943	0.7554	0.9536	1
11	0.4653	0.4977	0.6753	0.7065	0.7676	0.9536	1
12	0.4818	0.5196	0.6812	0.7164	0.7746	0.9536	1
13	0.493	0.5509	0.6943	0.7265	0.7718	0.9536	1
14	0.5071	0.5559	0.7065	0.7394	0.7874	0.9536	1
15	0.5234	0.5802	0.7227	0.7554	0.8037	0.9536	1
16	0.5489	0.6	0.733	0.7663	0.8318	0.9536	1
17	0.5639	0.6149	0.75	0.7831	0.8589	0.9536	1
18	0.5864	0.6456	0.7704	0.7947	0.8625	0.9536	1
19	0.6127	0.6603	0.7774	0.8113	0.8754	0.9536	1

Fig16.

X-axis values of Time (min)	Y-axis values of α, at 250 ^{0}C	Y-axis values of α, at 300 ^{0}C	Y-axis values of α, at 350 ^{0}C	Y-axis values of α, at 400 ^{0}C	Y-axis values of α, at 450 ^{0}C	Y-axis values of α, at 500 ^{0}C	Y-axis values of α, at 550 ^{0}C
0	0	0	0	0	0	0	0
1	0.2241	0.4631	0.4777	0.8973	0.9212	0.9314	1.0288
2	0.5239	0.621	0.8507	0.977	1.0218	1.1204	1.2826
3	0.6281	0.6996	0.9124	1.0631	1.111	1.2766	1.6136
4	0.7007	0.7932	0.973	1.1095	1.1791	1.5077	1.7366
5	0.7579	0.8677	1.0867	1.186	1.2628	1.7486	1.8157
6	0.817	0.9327	1.1791	1.2342	1.3469	1.7739	2.146
7	0.8763	0.9327	1.1946	1.2706	1.3678	2.146	2.146
8	0.9023	0.9533	1.2159	1.3011	1.3822	2.146	2.146
9	0.9199	0.977	1.255	1.3095	1.4204	2.146	2.146
10	0.9494	0.989	1.2512	1.3334	1.4533	2.146	2.146
11	0.969	1.0163	1.299	1.356	1.4796	2.146	2.146
12	0.9931	1.0486	1.3095	1.3749	1.495	2.146	2.146
13	1.0094	1.0957	1.3334	1.3946	1.4888	2.146	2.146
14	1.0302	1.1034	1.356	1.4204	1.5241	2.146	2.146
15	1.0544	1.141	1.3871	1.4533	1.5626	2.146	2.146
16	1.0927	1.1723	1.4073	1.4766	1.6351	2.146	2.146
17	1.1157	1.1964	1.442	1.5141	1.7139	2.146	2.146
18	1.1508	1.2474	1.4857	1.5412	1.7251	2.146	2.146
19	1.1929	1.2726	1.5013	1.5815	1.7674	2.146	2.146
20	1.2159	1.3289	1.5141	1.6221	1.8012	2.146	2.146

Fig17.

X-axis values of Time (min)	Y-axis values of α, at 550 ^{0}C	Y-axis values of α, at 500 ^{0}C	Y-axis values of α, at 450 ^{0}C	Y-axis values of α, at 400 ^{0}C	Y-axis values of α, at 350 ^{0}C	Y-axis values of α, at 300 ^{0}C
0	0	0	0	0	0	0
1	0.5305	0.3166	0.1969	0.1919	0.1562	0.1039
2	0.6312	0.6088	0.3755	0.205	0.1663	0.1061
3	0.7085	0.6934	0.4396	0.2517	0.1766	0.1334
4	0.7392	0.7085	0.4872	0.3166	0.1839	0.1556
5	0.7742	0.7225	0.5483	0.3755	0.1969	0.1821
6	0.7926	0.7392	0.5584	0.3893	0.2183	0.1919
7	0.8388	0.7551	0.5781	0.3958	0.2293	0.2
8	0.8696	0.7926	0.6101	0.4178	0.2463	0.2113
9	0.9051	0.8025	0.6436	0.4379	0.2517	0.226
10		0.8327	0.6838	0.4523	0.2692	0.2417
11		0.8586	0.749	0.4737	0.281	0.257
12		0.8658	0.7786	0.4911	0.2866	0.2713
13		0.8951	0.8239	0.5204	0.2929	0.2741
14		0.9293	0.8586	0.5506	0.2986	0.2789
15			0.886	0.5865	0.3108	0.2908
16			0.9106	0.6038	0.3218	0.3079
17			0.9684	0.6326	0.342	0.3137
18				0.6653	0.3558	0.3196
19				0.6838	0.3652	0.3218

20				0.712	0.3812	0.367
21				0.7243	0.4691	0.3831
22				0.7354	0.493	0.4025
23				0.7592	0.5431	0.4514
24				0.7926	0.5975	0.4596
25				0.8076	0.6326	0.4718
26					0.6638	0.4862
27					0.6967	0.498
28					0.7298	0.5101
29					0.7613	0.5407
30					0.7786	0.5584
31					0.7926	0.5781
32						0.595
33						0.6381
34						0.655
35						0.6791
36						0.728

Fig18.

X-axis values of Time (min)	Y-axis values of α, at 550 ^{0}C	Y-axis values of α, at 500 ^{0}C	Y-axis values of α, at 450 ^{0}C	Y-axis values of α, at 400 ^{0}C	Y-axis values of α, at 350 ^{0}C	Y-axis values of α, at 300 ^{0}C
0	0	0	0	0	0	0
1	1.2298	0.8726	0.6622	0.6528	0.5828	0.4684
2	1.4125	1.3702	0.9704	0.6774	0.6032	0.4737
3	1.5701	1.5377	1.0763	0.7615	0.6234	0.5351
4	1.6396	1.5701	1.1557	0.8726	0.6375	0.5816
5	1.7251	1.6012	1.2608	0.9704	0.6622	0.634
6	1.7739	1.6396	1.2786	0.9931	0.7019	0.6528
7	1.9104	1.6773	1.3138	1.0039	0.7217	0.668
8	2.0185	1.7739	1.3725	1.0401	0.7521	0.6891
9	2.1704	1.8012	1.4365	1.0733	0.7615	0.7159
10		1.8909	1.5174	1.0973	0.7921	0.7439
11		1.9779	1.6627	1.133	0.8122	0.7708
12		2.0043	1.7366	1.1623	0.8218	0.7956
13		2.1236	1.8638	1.2123	0.8326	0.8003
14		2.3018	1.9779	1.2647	0.8422	0.8087
15			2.0839	1.3289	0.8628	0.829
16			2.1973	1.3607	0.8812	0.8579
18				1.4796	0.9378	0.8775
19				1.5174	0.9734	0.8812
20				1.5672	1.2163	1.0463
21				1.6053	1.251	1.1095
22				1.6307	1.2963	1.1298
23				1.6874	1.357	1.154
24				1.7739	1.3491	1.174
25				1.8157	1.4151	1.1946
26					1.4766	1.2474
27					1.5447	1.2786
28					1.6178	1.3138
29					1.6925	1.3446
30					1.7366	1.4257
31					1.7739	1.459
32						1.5077
33						1.5342
34						1.559
35						1.6136
36						1.6533

4. CONCLUSION

TGA experiment of $BaC_2O_4.0.6H_2O$ and $FeC_2O_4.2H_2O$ (1:1) mole ratio mixture in air shows complete decomposition to BaO and Fe_2O_3 at 1000 ^{0}C through four well-defined steps while EGA technique shows decomposition to $BaCO_3$ and Fe_2O_3 at 1000 ^{0}C. The Ea values calculated from EGA are higher compared to those obtained from TGA method for the mixture due to the rate of reaction is hampered in close atmosphere. The non-isothermal TGA of $BaC_2O_4.0.6H_2O$ shows 80 % formation of BaO while in the $BaC_2O_4.0.6H_2O$ and $FeC_2O_4.2H_2O$ (1:1) mole ratio mixture shows 100% formation BaO this is due to the catalytic effect of Fe_2O_3. Intermediates, decomposition products as well as the final products were characterized by X-ray diffraction techniques. The increase in the intensity of the diffraction lines by raising the calcination temperature from 500 ^{0}C to 900 ^{0}C is attributed to the grain growth of the decomposition products. XRD experiments show the decomposition of $BaC_2O_4.0.6H_2O$ and $FeC_2O_4.2H_2O$ (1:1) mole ratio mixture to BaO and Fe_2O_3. The rate of reaction in TGA is controlled by the three dimentional diffusion (D_3) followed by random nucleation (Avrami equation) ($A_2\alpha$) while in EGA two dimensional phase boundary reaction ($R_2\alpha$) followed by random nucleation (Avrami equation) ($A_2\alpha$).

5. ACKNOWLEDGEMENT

The authors are grateful to the Head, Department of Chemistry and Principal, New Arts, Commerce and Science College, Ahmednagar for providing the all required facilities to carry out the work.

6. REFERENCES

1. Boldyrev, V. V, M. Bulens, M, and B. Delmon, B, "The Control of the reactivity of Solids" Elseveir, Amsterdam, (1979).
2. Nasr-Allah, M, Selim, M. M, Shahheen, W. M, "Effect of ZnO doping on surface and catalytic properties of manganese

oxides supported on alumina" *Materials Letters*., 52, 139–139 (2002).
3. Barbara. M, Drozdz-ciesla, E, Melecki, A, "Mechanism and kinetics of thermal decomposition of zinc oxalate" *Thermo-chemica. Acta*., 423, 13-18 (2004).
4. Gpalakrishnan, J, Sastri, M. V. C, Srinivasanand, V, Palanisamy, T, Viswanathan, B, "Kinetics of thermal decomposition of some metal oxalates" *Thermochimica. Acta*., 2, 265-273 (1971).
5. Brown, M. E, Coetzee, A, Eve, D. J, and Strydom. C. A, "Kinetics of the thermal dehydration and decomposition of some mixed metal oxalates" *Journal of Thermal Analysis.*, 41, 357–385 (1994).
6. Bhatta, D, Nayak, H, "Thermal analysis of La-Ba oxalate and role of γ-irradiation there on" *Thermochemica. Acta.*, 373, 37-43 (2001).
7. Górski, A, Kra´snicka, A. D, "The importance of the CO_2^{2-} anion in the mechanism of thermal decomposition of oxalates" *J. Therm. Anal. Calorim*., 32, 1229 – 1241(1987).
8. Bidaye, A. C, Majumdar, S, Sharma, I. G, Suri. A. K, "A study on isothermal kinetics of thermal decomposition of cobalt oxalate to cobalt " *Thermochim. Acta*., 473, 45–49 (2008).
9. Lingam, K. V, Rao, T. K. G, Reddy, M. V. V. S, "Radical studies in oxalate systems: E.S.R. of CO^{2-} in irradiated potassium oxalate monohydrate" *Mol. Phys*., 42, 1267–1269 (1981).
10. Leiga, A. G. "Decomposition of silver oxalate. II. Kinetics of the thermal decomposition" *J. Phys. Chem.* 70, 3260 – 3267 (1966).
11. Ganga Devi, T, Jose, J. M, Kannan, M. P, Muralidharan. K, "Effect of semiconducting metal oxide additives on the kinetics of thermal decomposition of sodium oxalate under isothermal conditions" *Thermochim. Acta*., 534, 71-76 (2012).
12. El-Bellihi, A. A, "Kinetics of the non-isothermal decomposition of Cu-and Co-itaconato complexes" *Journal of Thermal Analysis*., 41, 191–200 (1994).
13. Gabal, M. A, "Non-isothermal studies for the decomposition course of CdC_2O_4-ZnC_2O_4 mixture in Air" *Thermochemica. Acta*., 412, 55-62 (2004).
14. ARII, J. T. "Evolved gas analysis using photoionization mass spectrometry, EGA-PIMS: characterization of pyrolysis products from polymers" *Mass Spectrom. Soc. Jpn.*, 59 (1), 5–11 (2011).
15. Birzescu, M, Budru-geac, P, Dumitru, R, Niculescu, M, and Segal, E, "Copper (II) oxalate obtained through the reaction of 1, 2-ethanediol with Cu $(NO_3)2.3H_2O$" *Journal of Thermal Analysis and Calorimetry*., 94, 297 – 303 (2008).
16. International Centre for Diffraction Data, JCPDS, PDF2 Data Base Swarthmore, PA, USA., (1996).
17. Judd, M. D and Pope, M. I. "High temperature superconductivity 1: Materials" *Journal of Thermal Analysis*., 4, 31- 38 (1972).
18. Dollimore, D, Gao, X, "The thermal decomposition of oxalates: Patr26. A kinetic study of the thermal decomposition of manganese (II) oxalate dehydrate" *Thermochemica. Acta*., 215, 47 – 63 (1993).

19. Dong-Hua, C, Wan-Jun, T, "Thermal decomposition kinetics of ferrous oxalate dehydrate" *Acta Phys Chim Sin* 23 (04), 605 – 608 (2007).
20. Angermann, A, Topfer, J. "Synthesis of magnetite nanoparticles by thermal decomposition of ferrous oxalate dehydrate" *J. Mater Sci*., 43, 5123 – 5130 (2008).
21. Bhatti, A. S, Dollimore, D. "Thermal decomposition of oxalates. Part 19. The thermal decomposition of barium oxalate hemihydrates" *Themochimica. Acta.*, 79 (1), 217 – 230 (1984).
22. Bhatti, A. S, Dollimore, D, Fletcher, A, "Thermal decomposition of oxalates. Part 20. The decomposition kinetics of acid barium oxalates" *Themochimica. Acta.*, 79, 231- 241 (1984).
23. Bhatti, A. S, Diaz-Guemes, M. I, Dollimore. D. "Thermal decomposition of oxalates" *Themochimica. Acta*., 111, 275 – 282 (1987).
24. Jondo, T. K, Jorda, J. L, "Barium Oxides: Equilibrium and decomposition of BaO2" *Journal of Alloys and Compounds*., 327, 167 – 177 (2001).
25. Bandyopadhyay, N, Maitra, S. S, Roychoudhury, A. " Dehydration Kinetics of Ca-Aluminate Cement Hydrate Under Non-isothermal conditions" Ceramics international., 31, 371 – 374 (2005).
26. Gabal, M. A, "Kinetics of the thermal decomposition of CuC_2O_4 - ZnC_2O_4 mixture in air " *Thermochemica. Acta*., 402, 199 – 208 (2003).
27. Deb, N, "Thermal decomposition of manganese (II)bis (oxalate) Nickelate (II)tetrahydrate" *Journal of Themal Analysis and Calorimetry*., 81, 61- 65 (2005).
28. Muraleedharan, K and pasha, L. J. "Thermal decomposition of potassium titanium oxalate " *Serb. Chem. Soc*., 76 (7), 1015 – 1026 (2011).
29. Artini, C, Carnasciali, M. M, Costa, G. A, Masini, R, Ubaldini, A, "Thermal decomposition of mixed Ce and Gd oxalates and thermal properties of mixed Ce and Gd oxides" *Journal of Themal Analysis*., 84, 207 – 211 (2006).
30. Blesa, M. A, Domingo- Pascual, C, Jacobo, S. E, Rodriguez-Clemente, R, "Synthesis of ultrafine particles of barium ferrite by chemical coprecipitation" *Journal of Material Science.*, 32, 1025 – 1028 (1997).
31. Erchak Jr, M, Ward, R. "Catalytic properties of the products of the solid phase reaction between barium carbonate and ferric oxide" *J. Am. Chem. Soc.*, 68 (10), 2093 –2096 (1946).
32. Hermanek, M, Machala, Mashlan, M. L, Schnoeweiss, O, Zboril, R, "Thermal behavior of iron (II) oxalate dihydrate in the atmosphere of its conversion gases" *Journal of Material Chemistry*., 16, 1273 – 1280 (2006).
33. Choisnet, J and Raveau, B, "Evidence for partial cationic disorder in the $BaSrFe_4O_8$ type structure: the oxides$Ba_{2-x}Sr_xFe_4O_8$" *J. Mater. Chem*., 12, 1005-1008 (2002).
34. Hong, K. S, Shaheen, W. M, "Thermal characterization and physicochemical properties of Fe_2O_3-Mn_2O_3/Al_2O_3 system" *Thermochim. Acta*., 381, 153 – 164 (2002).
35. Boldyrev,V. V, "Thermal decomposition of silver oxalate" *Themochimica. Acta*., 388, 63 – 90 (2002).
36. Broadbent, D and Dollimore, J. "Kinetic study on the thermal decomposition of

copper(II) oxalate" *J. Chem. Soc. Faraday Trans*., 87, 161 – 166 (1991).

37. L'vov, B.V, "The interrelation between the temperature of solid decomposition and the E parameter of arrhenius equation" *Thermochim. Acta*., 389, 199 – 211 (2002).
38. Brown, M. E, Galwey, A. K, "Applications of the Arrhenius equation to solid state kinetics: can this be justified? " *Thermochim. Acta*., 386, 91 – 98 (2002).
39. Mathew, S, Nair, C. G. R, and Ninan, K. N, "Thermal decomposition kinetics.: part XVI. Kinetics and mechanism of thermal decomposition of diaquobis (ethylenediammine) copper (II) oxalate" *Thermochemica. Acta*., 150,63-78 (1989).